NASA TECHNICAL NOTE

NASA TN D-5160

c.1

NASA TN D-5160

THE LEADING-EDGE EFFECTS ON THE LAMINAR FLAT-PLATE BOUNDARY LAYER AND THE AERODYNAMIC HEATING AT MACH 10.4

by Howard W. Stone

Langley Research Center
Langley Station, Hampton, Va.

NATIONAL AERONAUTICS AND SPACE ADMINISTRATION • WASHINGTON, D. C. • MAY 1969

NASA TN D-5160

THE LEADING-EDGE EFFECTS ON THE LAMINAR FLAT-PLATE BOUNDARY LAYER AND THE AERODYNAMIC HEATING AT MACH 10.4

By Howard W. Stone

Langley Research Center
Langley Station, Hampton, Va.

NATIONAL AERONAUTICS AND SPACE ADMINISTRATION

For sale by the Clearinghouse for Federal Scientific and Technical Information
Springfield, Virginia 22151 – CFSTI price $3.00

THE LEADING-EDGE EFFECTS ON THE LAMINAR FLAT-PLATE BOUNDARY LAYER AND THE AERODYNAMIC HEATING AT MACH 10.4*

By Howard W. Stone
Langley Research Center

SUMMARY

Wall-pressure and heat-transfer distributions and boundary-layer impact-pressure profiles were obtained on a flat plate with both sharp and cylindrically blunted leading edges. The range of free-stream Reynolds number based on leading-edge thickness was from 73 to 70 000. Although the boundary-layer displacement effects behind a sharp leading edge are known to increase the wall pressure and heat transfer in the weak-interaction regime, these tests show that boundary-layer displacement effects result in only a slight change in the impact-pressure and velocity profiles. Slight blunting of the leading edge had little effect on the pressure distribution but, with the boundary layer growing in an entropy gradient, the heat transfer was reduced. Large leading-edge bluntness increased the heat transfer relative to the sharp leading edge.

INTRODUCTION

The effect of leading-edge thickness on the viscous flow field adjacent to a body in a hypersonic stream has been of interest to many researchers who have, in general, been concerned with the extremes of the problem; that is, the sharp leading edge or the very blunt leading edge. Experimental and theoretical studies of the sharp-leading-edge flat plate in a hypersonic flow with a laminar boundary layer are presented in references 1 to 4. The viscous-induced weak-interaction regime is discussed in references 1 to 3, whereas reference 4 reviews much of the work in the very near leading-edge regime. Experimental and theoretical studies for both the sharp-leading-edge and blunt-leading-edge flat plates with a laminar boundary layer are found in references 5 to 13. Generally, the wall-pressure distributions are reported to be in fair agreement with the various

*The material presented herein is based in part upon a thesis entitled "The Leading-Edge Effects on a Laminar Flat-Plate Boundary Layer at Mach 10.4" submitted in partial fulfillment of the requirements for the degree Master of Aerospace Engineering, University of Virginia, Charlottesville, Virginia, May 1968.

weak-interaction theories when the viscous-induced effects are predominant (sharp leading edge) and in fair agreement with the modified blast-wave theory when the inviscid effects are predominant (very blunt leading edge).

Measured laminar heat-transfer distributions for sharp- and blunt-leading-edge flat plates are presented in references 8 to 11. Bluntness generally tends to increase the heat transfer, but in reference 10 a slight decrease was shown prior to the increasing trend as the leading edge was progressively blunted.

Creager (ref. 14) conducted impact-pressure surveys of the region between the wall and the shock wave on flat plates with various leading-edge thicknesses at Mach 5.7. No attempt, however, was made to compare the surveys with theory.

The purpose of this investigation was to examine the leading-edge effect on the boundary-layer profiles and the boundary-layer thickness in addition to the wall pressures and heat transfer. These measurements were obtained on a flat plate behind a sharp leading edge and two blunt leading edges at a free-stream Mach number of 10.4. The impact-pressure profiles have been converted to velocity profiles and are compared with a zero-pressure-gradient boundary-layer solution and a boundary-layer theory using the local similarity concept to account for the effect of the pressure gradient. The tests were conducted in air with a range of free-stream Reynolds number based on leading-edge thickness from 73 to 70 000 for leading-edge thicknesses of 0.005, 0.16, and 1.27 cm.

SYMBOLS

a speed of sound

C_m heat capacity of the metal

$C_w = \frac{\mu_w}{\mu_\infty} \frac{T_\infty}{T_w}$

d leading-edge diameter

h enthalpy

K_3 pressure gradient correction factor (see ref. 12)

M Mach number

$N_{St,\infty}$ Stanton number based on free-stream conditions

p	pressure
$p_{t,2}$	impact pressure
R_∞/x	unit Reynolds number based on free-stream conditions
$R_{\infty,d}$	Reynolds number based on free-stream conditions and leading-edge diameter
$R_{\infty,x}$	Reynolds number based on free-stream conditions and distance from leading edge
T	temperature
u	velocity
u'	effective velocity
x	distance from leading edge of sharp model
y	distance perpendicular to model surface
z	lateral distance on model surface measured from model center line
γ	ratio of specific heats
δ	boundary-layer thickness
δ'	boundary-layer characteristic thickness
η_∞	Blasius similarity variable, $\frac{y}{x}\sqrt{R_{\infty,x}}$
μ	viscosity

$$\overline{\chi}_\infty = \frac{M_\infty{}^3\sqrt{C_w}}{\sqrt{R_{\infty,x}}}$$

Subscripts:

e	boundary-layer-edge condition

t	total (stagnation) condition
w	wall condition
∞	free-stream condition

APPARATUS AND TESTS

Facility and Test Conditions

The present tests were conducted in the Mach 10 test section of the Langley continuous-flow hypersonic tunnel. In this facility the prescribed test conditions are continuously maintained in the 79-cm-square test section by recirculating the test air through a series of compressors and electrical resistance tube heaters which heat the test air to avoid liquefaction. A more complete description of the facility is available in reference 15.

The tunnel Mach number distributions obtained from impact-pressure surveys are presented in figure 1 for the nominal test stagnation chamber pressures of this study. The nominal test conditions obtained by assuming an isentropic expansion (with corrections for intermolecular force effects, ref. 16) are summarized in the following table:

p_t, kN/m^2	M_∞	Free-stream unit Reynolds number per cm, R_∞/x
2410	10.3	1.5×10^4
5170	10.4	3.1
8270	10.4	5.1

The maximum deviation from the nominal test stagnation-pressure values for different runs was 0.8 percent whereas the test stagnation temperatures varied from 966° K to 1040° K with no more than an 8° variation during a given run. These deviations in the stagnation conditions along with slight tunnel Mach number gradients result in a Mach number deviation of ± 0.10.

Models and Instrumentation

The flat-plate models consisted of interchangeable instrumented plates supported by a frame with a 20° bevel extending across the leading edge and along both sides of the plate. (See fig. 2.) The pressure plate was 0.476-cm-thick stainless steel with 0.178-cm pressure orifices located as shown in figure 3. The wall-pressure measurements at

36 orifices were obtained by three ionization gages connected through three 12-port scanning valves. All the data were recorded automatically on magnetic tape by an analog-to-digital converter. Random instrument errors plus recording errors result in an accuracy of about ±6 percent of reading.

The measured mean thickness of the inconel heat-transfer plate was 0.081 cm ±5 percent. The material density was 8.41×10^3 kg/m^3 and from a curve fit of values published in the literature, the heat capacity in J/g-$^{\circ}$K varied as

$$C_m = \left[0.0000611\left(\frac{9T_w}{5} - 460\right) + 0.0980\right]4.187 \qquad (1)$$

The temperature on the back side of the thin inconel plate was measured by 30-gage chromel-alumel thermocouples spotwelded to the plate at the locations shown in figure 4.

The leading edges of the sharp plates were 0.005 ± 0.002 cm thick and were modified by adding cylindrical leading edges 0.16 cm and 1.27 cm in diameter for the blunt-model tests. Both the heat-transfer plate and the pressure plates had mirror finishes with a maximum waviness of 0.33° on the center line. Detachable end plates with sharp leading edges were constructed from 0.32-cm-thick stainless steel. The shape of the end plate is shown in figure 4.

Boundary-Layer Probes

Two boundary-layer probes were constructed for these tests. Each probe had three tubes formed from stainless-steel tubing having 0.23-cm i.d. and 0.32-cm o.d. which was flattened and filed at the tip to form almost rectangular orifices. The three tubes were mounted on a 1.27-cm o.d. stainless tube which was air-cooled. A sketch of the probe heads and the measurements of each orifice are presented in figure 5. A photograph of one of the probes is shown as figure 6.

The tube heights were less than 15 percent of the expected minimum boundary-layer thickness which is consistent with criteria obtained from previous probe work (e.g., refs. 2 and 17). Also, the tubes were flattened to a width-height ratio of approximately 7 after the "viscous effect" study of MacMillan (ref. 18).

Both probes were electrically driven from outside the tunnel. During bench tests of the traversing mechanisms, the probe location always repeated to within 0.008 cm when within 2.5 cm of the model surface. The surveys were conducted at the locations shown in figure 3. Each tube of the boundary-layer probes was connected to multiple transducers to provide an accuracy of ±3 percent over the range of impact pressures incurred.

Tests

In all tests, the model was injected into the tunnel in less than 1 second after the proper test conditions had been established, and the desired data were measured. Upon completion of these measurements, the model was withdrawn from the stream and cooled by air jets to nearly room temperature. Oil-flow tests were conducted on the sharp-leading-edge model initially to establish which end-plate configuration would provide parallel flow on the model center line. In the wall-pressure tests and the boundary-layer surveys, the pressures were monitored continuously and were recorded on magnetic tape after they had reached steady state. During the surveys, when the probe touched the model surface the fouling circuit signaled and a data point was recorded to establish the surface location on the recorded data. The probe was moved only in the direction toward the model surface throughout all surveys. In the heat-transfer tests, the temperature at each thermocouple was recorded 20 times per second for about 5 seconds. The Stanton number was obtained by applying the transient-calorimeter technique which involves calculating the rate of heat storage in the thin metal skin from the slope of the measured temperature-time data as described in reference 15. In the present tests, free-stream flow properties were used throughout the calculation.

DISCUSSION OF RESULTS

In this investigation, an end plate was installed on the strut side of the model and extended upward at an angle of 30° to the plane of the model surface. In this configuration, the model surface was shielded from the interference field of the strut. The oil-flow pattern (see fig. 7) shows that except for a slight inward flow near the leading edge on the far side and some outward flow along the sides, the flow over the plate was parallel to the center line. The spanwise pressures for this configuration at the 90-percent-chord location were constant within the accuracy of the data.

Pressure Distributions

The bluntness and viscous-interaction effects on the wall-pressure distributions are shown in figure 8 where p_w/p_∞ along the model center line is plotted as a function of x for three unit Reynolds numbers. The modified blast-wave theory of Bertram and Blackstock (ref. 13) is generally in good agreement with the pressures behind the 1.27-cm-diameter leading edge where the bluntness-induced effects are dominant. There is, however, some difference between data and theory on the rear of the model due probably to transducer inaccuracy. The data for the models with the 0.16-cm-diameter and the sharp leading edges agree almost within the accuracy of the data.

The wall pressures for the models with the sharp- and 0.16-cm-diameter leading edges tend to increase slightly on the rear third of the model but the oil-flow patterns and the lateral pressure distributions did not indicate any model edge effects in this region. There does appear to be a model trailing-edge effect over the last 5 cm of the model.

The "complete" theory of Bertram and Blackstock (iteration of eqs. (7) and (15) of ref. 13) for predicting viscous-induced pressures, shown in figure 8, does not predict the sharp-leading-edge data. The theory assumes an isothermal wall $\left(T_w/T_t \approx 0.34 \text{ in the present tests}\right)$ but the temperature of the leading edge itself will approach the stream total temperature which may have an effect on boundary-layer growth and thus on the induced pressure rise. Also a slight misalinement of the model with respect to the tunnel flow may account for most of this difference at the highest unit Reynolds number; however, the greater part of the difference at the lower unit Reynolds number is unexplained.

Impact-Pressure Profiles

Changes in the boundary layer and the adjacent flow field due to changing the leading-edge thickness are shown in the measured impact-pressure profiles presented in figure 9. Comparison of the impact-pressure profiles for the models with the sharp- and the 0.16-cm-diameter leading edges reveal a marked leading-edge effect whereas the wall-pressure distributions were very similar. The profiles at $x = 71.6$ cm for the 1.27-cm-diameter leading-edge model (fig. 9(c)) were reduced by using the blast-wave values of p_w instead of the measured values. The profiles at both probe locations for the 1.27-cm-diameter leading-edge model agree outside of the boundary layer where the impact pressures were equal to the values calculated by assuming an isentropic expansion from the model stagnation line. Thus, the boundary layer behind the 1.27-cm-diameter leading edge grew in a region of constant entropy associated with the normal portion of the bow shock wave.

Velocity Profiles

The velocity profiles for the sharp-leading-edge model at each unit Reynolds number are presented in figure 10. These data were obtained from the measured impact-pressure profiles by using a theoretical total-enthalpy distribution due to the theory of Klunker and McLean from reference 19 (discussed in the appendix). As the figure shows, the near-wall data points are affected by the wall-probe interaction and possibly by the low Reynolds number effect. These data points are neglected, therefore, throughout the rest of the discussion. The theory of Klunker and McLean and the data are in good agreement at all Reynolds numbers. Thus, a zero-pressure-gradient boundary-layer theory

based on free-stream conditions will provide, for these test conditions, a satisfactory estimate of the boundary-layer characteristics for $0.57 \leqq \overline{\chi}_\infty \leqq 1.38$ which is assumed in the weak-interaction theory.

The wall pressures on the sharp-leading-edge model are in a range where the measurements presented in reference 20 show that there is a small effect of low pressure on the viscosity. Therefore, the Klunker and McLean theory was also calculated using the Kurdt and Warberg equation (ref. 20) for the variation of viscosity with pressure. The resulting theoretical velocity profiles were only slightly different from the theoretical velocity profiles presented in figure 10.

The velocity profiles for the 0.16-cm-diameter leading-edge model, taken at 94 and 176 diameters from the leading edge, are presented in figure 11 along with the profiles of the Klunker and McLean theory for a sharp leading edge for comparison. The theory also provided the total-enthalpy distribution that was used to obtain the velocity from the measured data. The data show that there is a small velocity gradient outside of the boundary layer. In figure 11(a), for $x = 38.1$ cm, the "knee" of the profile normally associated with the boundary-layer edge appears to be at $\eta_\infty = 32$. This location corresponds to $y = 1.53$ cm on the impact-pressure profiles presented in figure 9(b) or $\left(p_{t,2}/p_w\right)_e$ is approximately 27 at the boundary-layer edge. The impact-pressure gradient outside of the boundary layer indicates that the boundary layer is growing in an entropy gradient.

Behind the 1.27-cm-diameter leading edge, the boundary layer has been shown to be growing in the region of constant entropy adjacent to the model surface. The local similarity theory discussed in the appendix was used to calculate velocity profiles for this configuration by assuming that the Mach 10.4 normal-shock total pressure was the boundary-layer-edge total pressure. The velocity profiles were computed from the measured impact-pressure data by using the total-enthalpy distribution calculated by the local similarity theory. The theory and the velocity-profile data shown in figure 12 are in good agreement at $x = 38.1$ cm but do not agree as well at $x = 71.6$ cm.

To obtain an indication of the bluntness effect on the velocity profiles, a boundary-layer characteristic thickness δ' was defined as the point where a straight-line fairing of the linear portion of the boundary-layer velocity profile crosses a straight-line fairing of the velocity data points outside of the boundary layer. This point also defines an effective boundary-layer edge velocity u'_e. A plot of u/u'_e as a function of y/δ' for the three leading-edge configurations is presented in figure 13. The bluntness effect is confined to the outer portion of the boundary layer where the boundary layer is thickened and the velocity gradient decreased as the leading-edge thickness is increased.

Heat Transfer

The heat-transfer data, presented in figure 14, show that progressively blunting the leading edge first decreases and then increases the wall heat transfer relative to that for the sharp-leading-edge model. Neal (ref. 10) found a similar bluntness effect at $M_\infty = 6.8$.

The results of the Bertram and Feller (ref. 12) method to "correct" the heat-transfer data for the effect of the induced pressures are shown in figure 15. Both the "corrected" and "uncorrected" heat-transfer data for the sharp-leading-edge model are compared with the zero-pressure-gradient theory of Klunker and McLean. The fairing through the uncorrected data is parallel to and 19 percent above the theory. There is good agreement between the corrected data and the theory.

Boundary-Layer Thickness

Creager (ref. 21) found fair agreement between his $M_\infty = 4.0$ boundary-layer-thickness data and the equation

$$\frac{\delta}{d}\sqrt{R_{\infty,d}} = \left[\frac{1.73}{M_\infty{}^2}\left(\frac{T_w}{T_\infty}\right) + 0.332(\gamma - 1) + \frac{4.27}{M_\infty{}^2}\right] M_\infty{}^2 \sqrt{C_w}\sqrt{\frac{x}{d}} \tag{2}$$

Comparison of the present test results with this equation required locating the boundary-layer edge, usually defined as the location of $u/u_e = 0.999$. However, this definition is difficult to apply to the intermediate bluntness profiles with the velocity gradient outside the boundary layer. In an attempt to select a comparable boundary-layer edge value, a straight-line fairing of the velocity data outside the boundary layer was assumed to be analogous to the $u/u_e = 1.0$ line. The tangent point of the data with this fairing was selected as the boundary-layer edge. These data are compared with a plot of equation (2) in figure 16. The Monaghan T' prediction (ref. 22) based on the free-stream conditions is also shown in the figure. Both methods provide a satisfactory estimate of the boundary-layer thickness for the sharp- and 1.27-cm-diameter leading-edge data and a portion of the 0.16-cm-diameter leading-edge data. Creager's data (ref. 21) showed that the boundary-layer thickness is proportional to the square root of x for $0.6 \leqq \frac{x}{d} \leqq 15.5$ at Mach 4. The present data show that $\delta \propto \sqrt{x}$ for $30 \leqq \frac{x}{d} \leqq 14\,000$ at Mach 10.4.

CONCLUSIONS

The investigation of the leading-edge effects on the laminar boundary layer of a flat plate with a sharp and two cylindrically blunted leading edges in a Mach 10.4 airstream support the following conclusions:

1. The boundary-layer solution presented in NACA TN 2916, based on the assumption of a constant wall pressure, was in good agreement with the velocity-profile data for the sharp flat plate with a weak-interaction wall-pressure distribution. The heat-transfer data agreed with the theory after a modification for the wall pressures by the method presented in NASA MEMO 5-24-59L.

2. The profile data for the 0.16-cm-diameter leading-edge model, taken at 94 and 176 diameters from the leading edge, indicated that a large impact-pressure gradient and a small velocity gradient existed outside the boundary; that is, the boundary layer was growing in an entropy gradient. This bluntness thickened the boundary layer and slightly reduced the heat-transfer coefficients relative to the sharp-leading-edge data.

3. The velocity-profile data for the 1.27-cm-diameter leading-edge model were in fair agreement with a local similarity boundary-layer theory. The large bluntness increased the heat-transfer coefficients relative to the data for the sharp-leading-edge model.

Langley Research Center,
National Aeronautics and Space Administration,
Langley Station, Hampton, Va., February 14, 1969,
129-01-07-07-23.

APPENDIX

ANALYTICAL METHODS

Laminar Boundary-Layer Theories

The theory of Klunker and McLean (ref. 19) is an easily programed iterative solution for the two-dimensional compressible laminar boundary-layer equations in the absence of a pressure gradient and for an isothermal wall. The solution includes the temperature variation of all fluid thermal properties, and the results are representative of the constant-pressure solutions for a flat plate. The Blasius similarity parameter is used to reduce the boundary-layer equations for steady flow along an isothermal wall to total differential equations. After the equations are nondimensionalized and simplified by integrating factors, a rapidly converging, successive approximation, integration method is used to obtain a solution. In the present application the fluid thermal properties are obtained from the NBS tables (ref. 23). The work of Grieser and Goldthwaite (ref. 20) is used to evaluate the viscosity. The equation for viscosity in N-sec/m^2

$$\mu = 1.419 \frac{T^{3/2}}{T + 99.22} \times 10^{-6} \tag{A1}$$

represents the best fit of their data over the temperature range from 80° to 294° R. In the present investigation the free-stream conditions were used throughout the solution.

The local similarity concept can be used to account for the effect of the pressure gradient on the boundary layer. A programed numerical solution for the locally similar equations of reference 24 was used to obtain theoretical estimates in this investigation. The solution used was for an ideal gas with a Sutherland law form of viscosity variation. This solution requires prior knowledge of the boundary-layer edge flow properties and, therefore, can be used satisfactorily only when the static- and total-pressure distributions are known over the entire length of the model. The wall was assumed to be isothermal.

Total-Enthalpy Profiles

To obtain velocity profiles from the measured impact-pressure profiles, it is necessary to know the corresponding total-temperature or total-enthalpy profile. Unfortunately, there was no reliable total-temperature probe available that could be used in these tests at the time the tests were performed and, therefore, an appropriate theoretical profile was used. Any error due to this assumption is reduced in the velocity profiles, however, since the velocity is proportional to the square root of the difference between the total and static enthalpy and the values are fixed where the difference approaches zero.

APPENDIX

The calculation procedure involved applying the energy equation

$$h_t = h + \frac{M^2 a^2}{2} \tag{A2}$$

to each data point in the boundary-layer profile. At each point M was known from the measured profile and an appropriate value of h_t was known from the assumed total-enthalpy distribution. Equation (A2) can be solved either by assuming an ideal gas and using the appropriate definitions of h and a or by an interation procedure using tables of values of h and a as a function of temperature such as the NBS tables (ref. 23). Both procedures were used and yield almost the same results for the conditions of the present tests.

REFERENCES

1. Lees, Lester; and Probstein, Ronald R.: Hypersonic Viscous Flow Over a Flat Plate. Rep. No. 195 (Contract AF 33(038)-250), Aeronaut. Eng. Lab., Princeton Univ., Apr. 20, 1952.

2. Kendall, James M., Jr.: An Experimental Investigation of Leading-Edge Shock-Wave – Boundary-Layer Interaction at Mach 5.8. J. Aeronaut. Sci., vol. 24, no. 1, Jan. 1957, pp. 47-56.

3. Bertram, Mitchel H.: Boundary-Layer Displacement Effects in Air at Mach Numbers of 6.8 and 9.6. NASA TR R-22, 1959. (Supersedes NACA TN 4133.)

4. Moulic, E. S., Jr.: Local Skin Friction and Induced Pressure Measurements on a Sharp-Edged Insulated Flat Plate in Low Density Hypersonic Flow. Tech. Rep. (Grant NSF GP-2520), Ser. 7, Issue No. 3, Space Sci. Lab., Univ. of California, Jan. 10, 1966.

5. Lees, Lester: Inviscid Hypersonic Flow Over Blunt-Nosed Slender Bodies. GALCIT Hypersonic Res. Proj. Mem. No. 31 (Contract No. DA-04-495-Ord-19), Feb. 1, 1956.

6. Cheng, H. K.; Hall, J. Gordon; Golian, T. C.; and Hertzberg, A.: Boundary-Layer Displacement and Leading-Edge Bluntness Effects in High-Temperature Hypersonic Flow. J. Aerosp. Sci., vol. 28, no. 5, May 1961, pp. 353-381, 410.

7. Graham, W. J.; and Vas, I. E.: The Effect of Leading Edge Conditions on the Detailed Flow Over a Flat Plate at $M = 11.7$. ARL 138, U.S. Air Force, Sept. 1961.

8. Marvin, Joseph G.: Surface Pressures and Heat Transfer on Unswept Blunt Plates in Helium at High Mach Numbers. NASA TN D-688, 1961.

9. Harvey, William D.: Effects of Leading-Edge Bluntness on Pressure and Heat-Transfer Measurements Over a Flat Plate at a Mach Number of 20. NASA TN D-2846, 1965.

10. Neal, Luther, Jr.: A Study of the Pressure, Heat Transfer, and Skin Friction on Sharp and Blunt Flat Plates at Mach 6.8. NASA TN D-3312, 1966.

11. Townsend, J. C.; Vollmar, W. R.; and Vas, I. E.: The Leading Edge Effect on the Flow Over a Flat Plate at $M = 10$. Rep. ARL 66-0145 (Contract AF 33(616)-7629), Dep. Aerosp. Mech. Sci., Princeton Univ., July 1966. (Available from DDC as AD 642436.)

12. Bertram, Mitchel H.; and Feller, William V.: A Simple Method for Determining Heat Transfer, Skin Friction, and Boundary-Layer Thickness for Hypersonic Laminar Boundary-Layer Flows in a Pressure Gradient. NASA MEMO 5-24-59L, 1959.

13. Bertram, Mitchel H.; and Blackstock, Thomas A.: Some Simple Solutions to the Problem of Predicting Boundary-Layer Self-Induced Pressures. NASA TN D-798, 1961.

14. Creager, Marcus O.: Effect of Leading-Edge Thickness on the Flow Over a Flat Plate at a Mach Number of 5.7. NASA TN D-313, 1960.

15. Dunavant, James C.; and Stone, Howard W.: Effect of Roughness on Heat Transfer to Hemisphere Cylinders at Mach Numbers 10.4 and 11.4. NASA TN D-3871, 1967.

16. Erickson, Wayne D.; and Creekmore, Helen S.: A Study of Equilibrium Real-Gas Effects in Hypersonic Air Nozzles, Including Charts of Thermodynamic Properties for Equilibrium Air. NASA TN D-231, 1960.

17. Bradfield, W. S.; DeCoursin, D. G.; and Blumer, C. B.: The Effect of Leading-Edge Bluntness on a Laminar Supersonic Boundary Layer. J. Aeronaut. Sci., vol. 21, no. 6, June 1954, pp. 373-382, 398.

18. MacMillan, F. A.: Viscous Effects on Flattened Pitot Tubes at Low Speeds. J. Roy. Aeronaut. Soc. (Tech. Notes), vol. 58, no. 528, Dec. 1954, pp. 837-839.

19. Klunker, E. B.; and McLean, F. Edward: Effect of Thermal Properties on Laminar-Boundary-Layer Characteristics. NACA TN 2916, 1953.

20. Grieser, Daniel R.; and Goldthwaite, William H.: Experimental Determination of the Viscosity of Air in the Gaseous State at Low Temperatures and Pressures. AEDC-TDR-63-143, U.S. Air Force, June 1963.

21. Creager, Marcus O.: Effects of Leading-Edge Blunting on the Local Heat Transfer and Pressure Distributions Over Flat Plates in Supersonic Flow. NACA TN 4142, 1957.

22. Monaghan, R. J.: An Approximate Solution of the Compressible Laminar Boundary Layer on a Flat Plate. R. & M. No. 2760, Brit. A.R.C., 1953.

23. Hilsenrath, Joseph; Beckett, Charles W., et al.: Tables of Thermal Properties of Gases. NBS Circ. 564, U.S. Dep. of Com., 1955.

24. Cohen, Nathaniel B.: Boundary-Layer Similar Solutions and Correlation Equations for Laminar Heat-Transfer Distribution in Equilibrium Air at Velocities up to 41,100 Feet Per Second. NASA TR R-118, 1961.

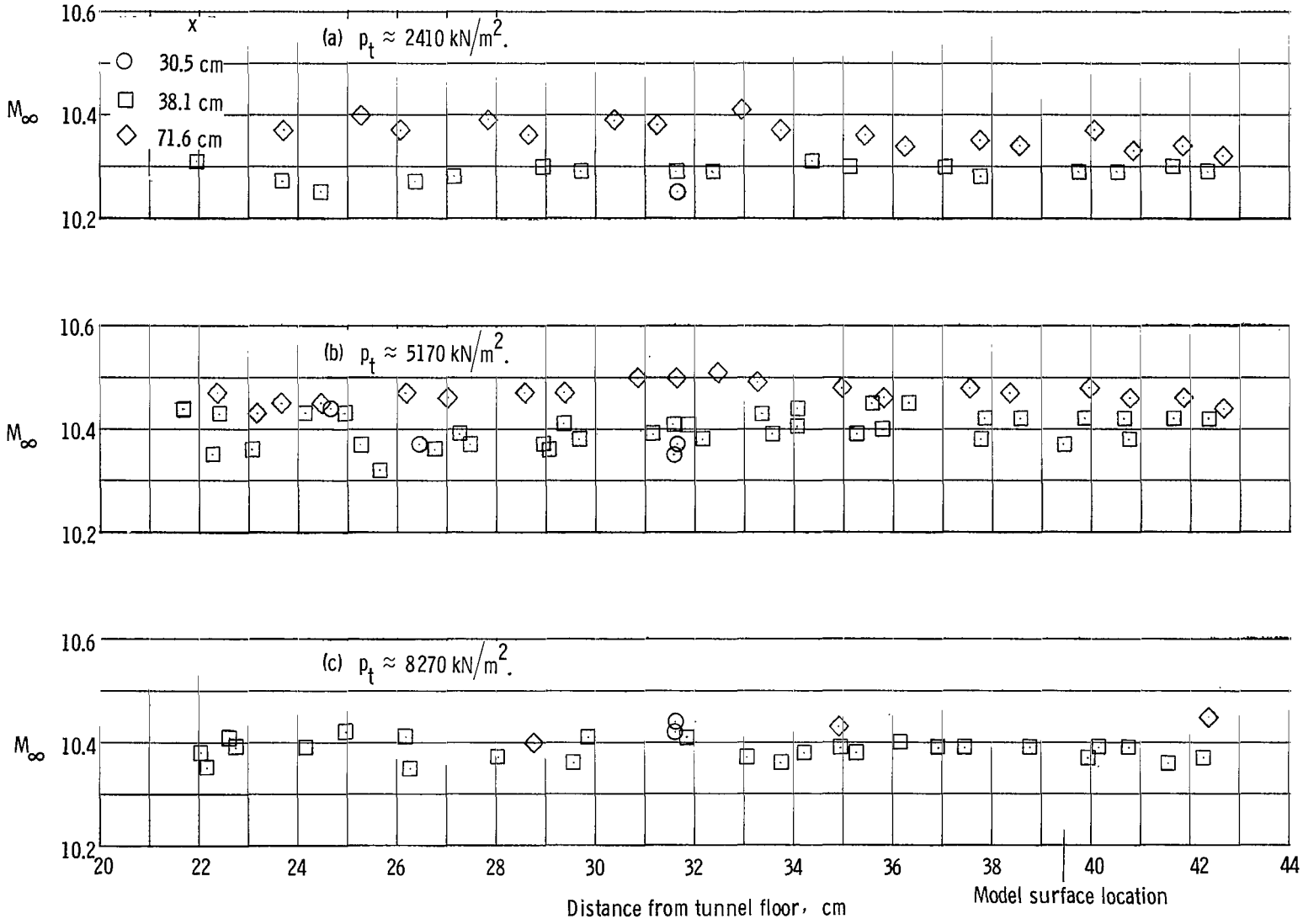

Figure 1.- Tunnel Mach number calibration.

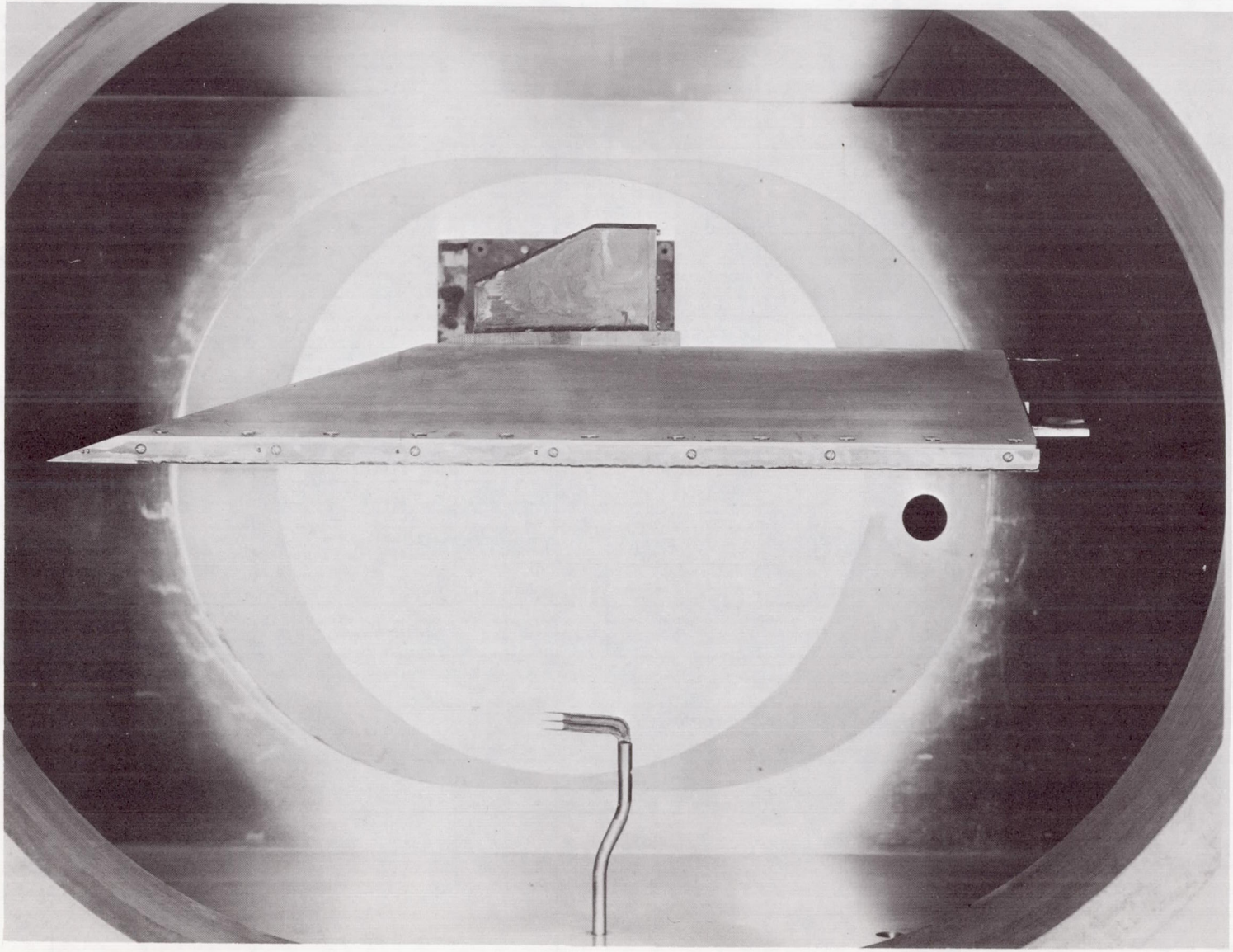

Figure 2.- Model positioned in test section. L-65-5823

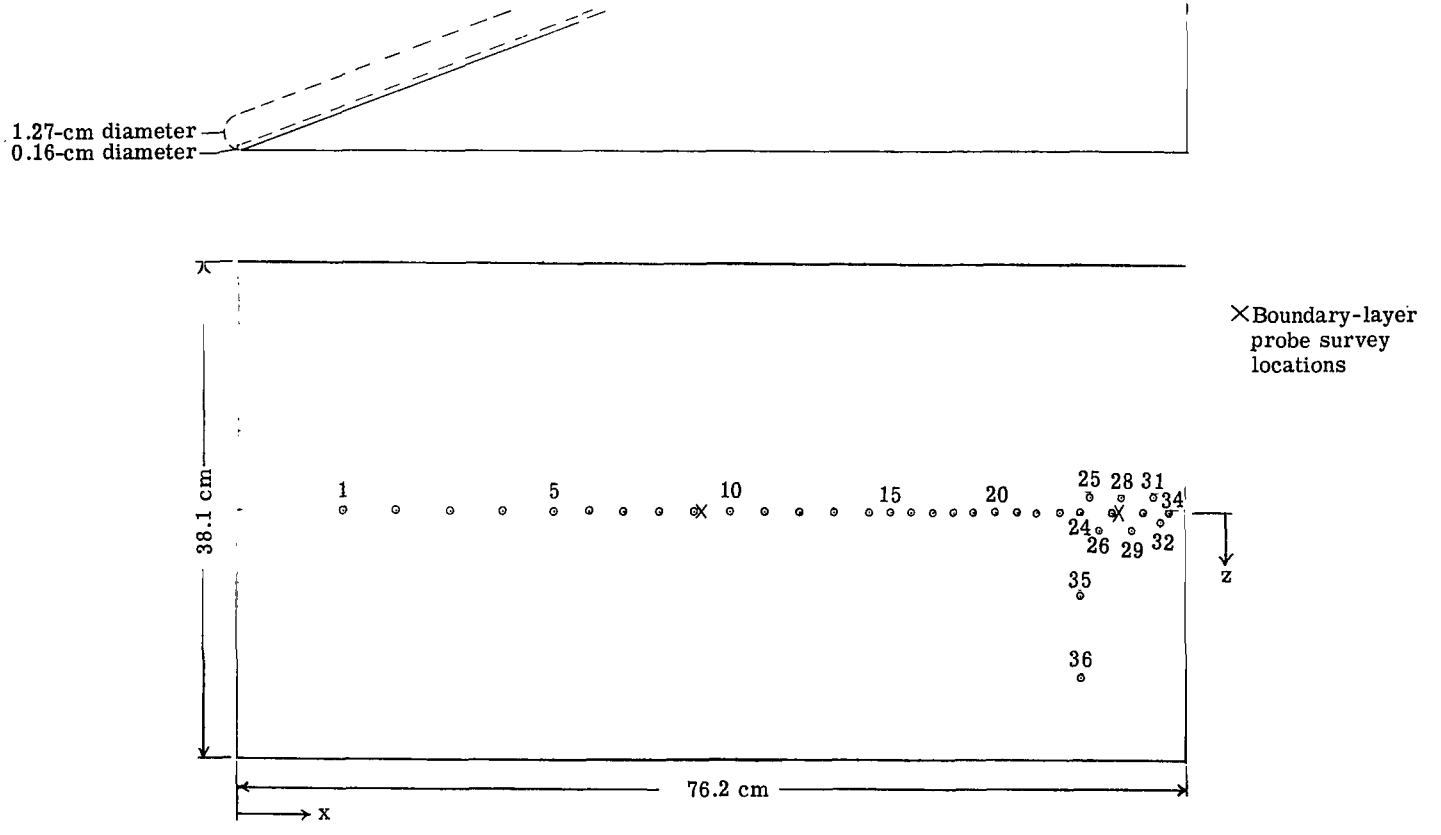

Location of Pressure Tubes											
No.	x	z	No.	x	z	No.	x	z	No.	x	z
1	9.78	0	10	39.50	0	19	59.26	0	28	71.12	+1.27
2	14.02	0	11	42.32	0	20	60.96	0	29	71.96	-1.27
3	18.24	0	12	45.14	0	21	62.64	0	30	72.80	0
4	22.48	0	13	47.96	0	22	64.34	0	31	73.66	+1.27
5	25.40	0	14	50.80	0	23	66.04	0	32	74.30	-.64
6	28.21	0	15	52.48	0	24	67.72	0	33	74.93	0
7	31.04	0	16	54.18	0	25	68.58	+1.27	34	75.56	+.64
8	33.85	0	17	55.88	0	26	69.41	-1.27	35	67.72	-.64
9	36.67	0	18	57.56	0	27	70.26	0	36	67.72	-12.70

Figure 3.- Pressure-orifice and boundary-layer probe survey locations. All dimensions are in centimeters.

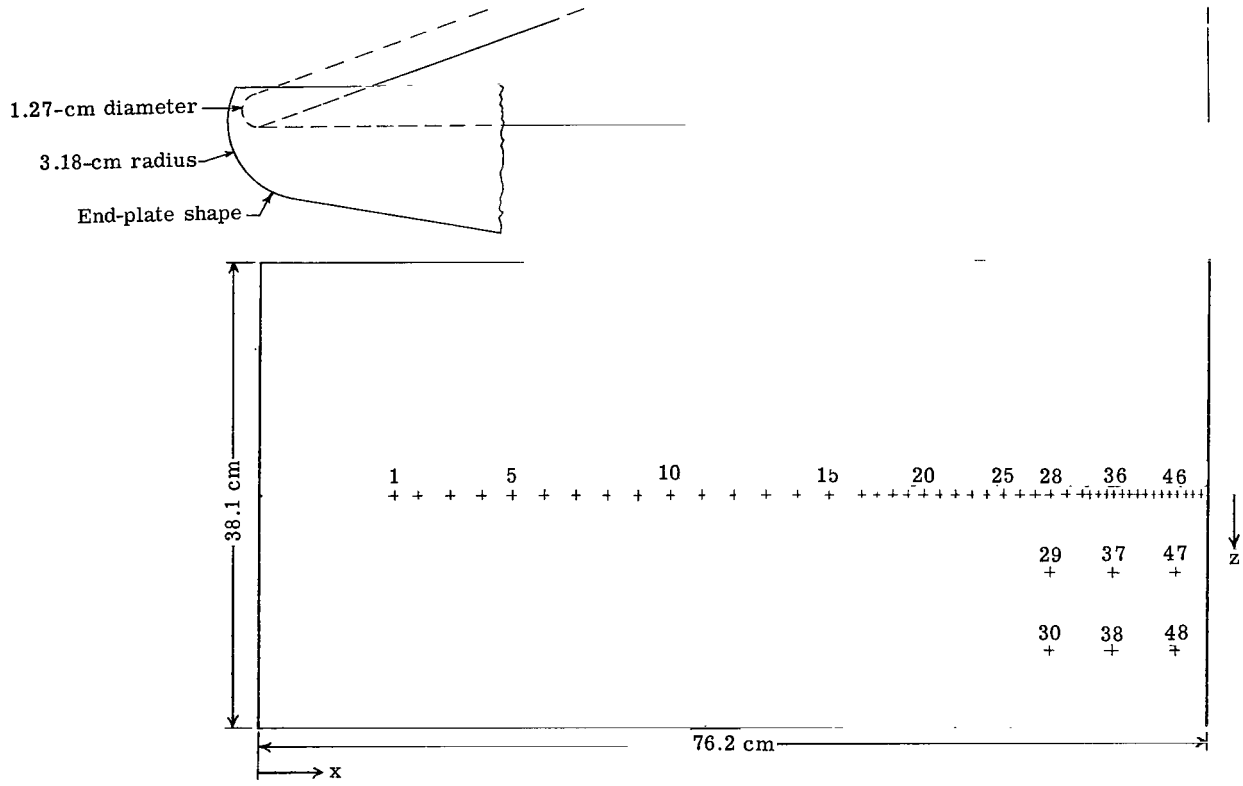

Thermocouple Position											
No.	x	z	No.	x	z	No.	x	z	No.	x	z
1	10.80	0	14	43.18	0	27	62.23	0	40	69.85	0
2	12.70	0	15	45.72	0	28	63.50	0	41	70.48	0
3	15.24	0	16	48.26	0	29	63.50	6.35	42	71.12	0
4	17.78	0	17	49.53	0	30	63.50	12.70	43	71.76	0
5	20.32	0	18	50.80	0	31	64.77	0	44	72.39	0
6	22.86	0	19	52.07	0	32	66.04	0	45	73.02	0
7	25.40	0	20	53.34	0	33	66.68	0	46	73.66	0
8	27.94	0	21	54.61	0	34	67.31	0	47	73.66	6.35
9	30.48	0	22	55.88	0	35	67.94	0	48	73.66	12.70
10	33.02	0	23	57.15	0	36	68.58	0	49	74.30	0
11	35.56	0	24	58.42	0	37	68.58	6.35	50	74.93	0
12	38.10	0	25	59.69	0	38	68.58	12.70	51	75.56	0
13	40.64	0	26	60.96	0	39	69.22	0			

Figure 4.- Thermocouple locations and end-plate shape. All dimensions are in centimeters.

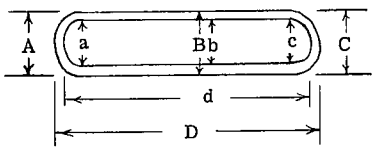

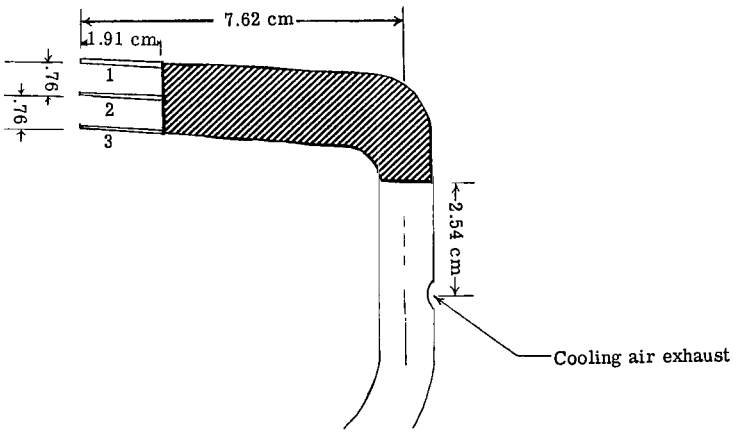

	Probe No. 1				Probe No. 2		
	Tube 1	Tube 2	Tube 3		Tube 1	Tube 2	Tube 3
A	0.051	0.053	0.053	A	0.046	0.053	0.533
a	.033	.003	.031	a	.033	.031	.025
B	.058	.081	.061	B	.051	.053	.056
b	.028	.028	.028	b	.031	.031	.025
C	.051	.051	.056	C	.048	.046	.051
c	.031	.033	.036	c	.033	.028	.023
D	.386	.391	.396	D	.412	.409	.409
d	.345	.353	.356	d	.356	.348	.361

Figure 5.- Sketch of boundary-layer probe heads. All dimensions are in centimeters.

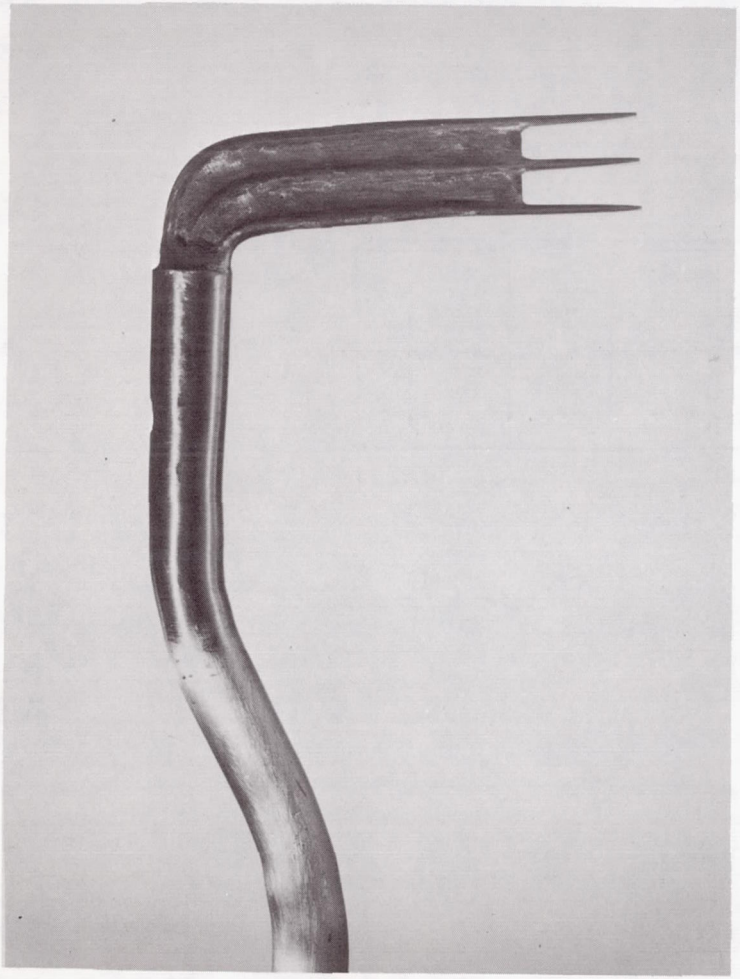

L-65-1672

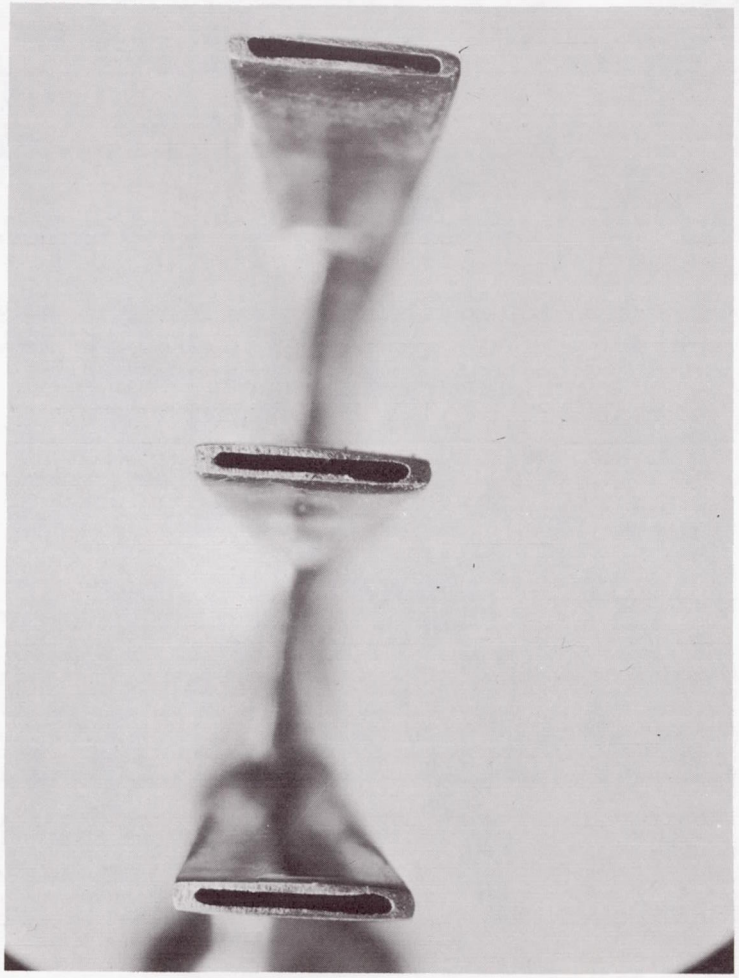

L-65-1673

Figure 6.- Photographs of boundary-layer probe head.

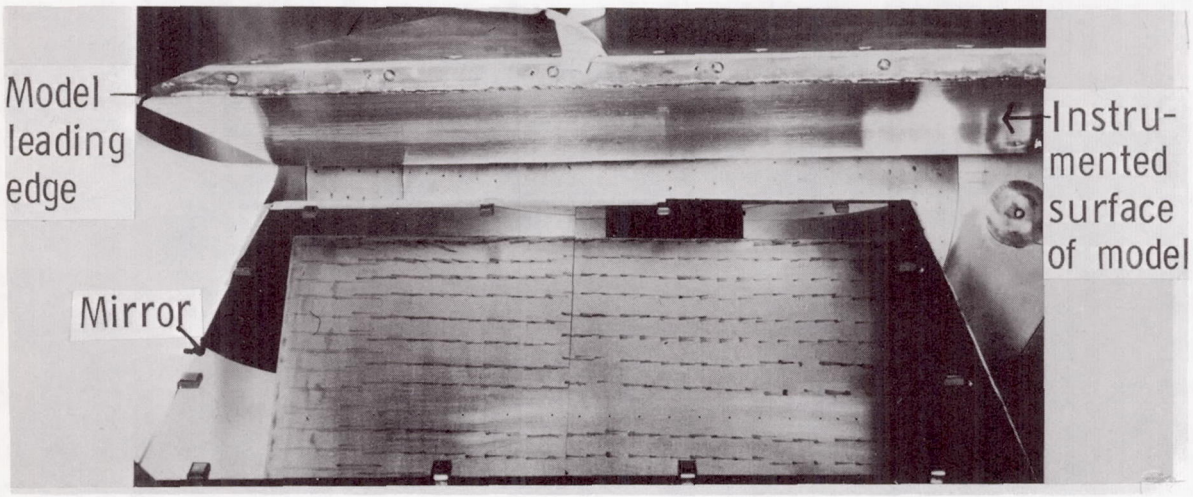

Front portion of model

L-65-6251.1

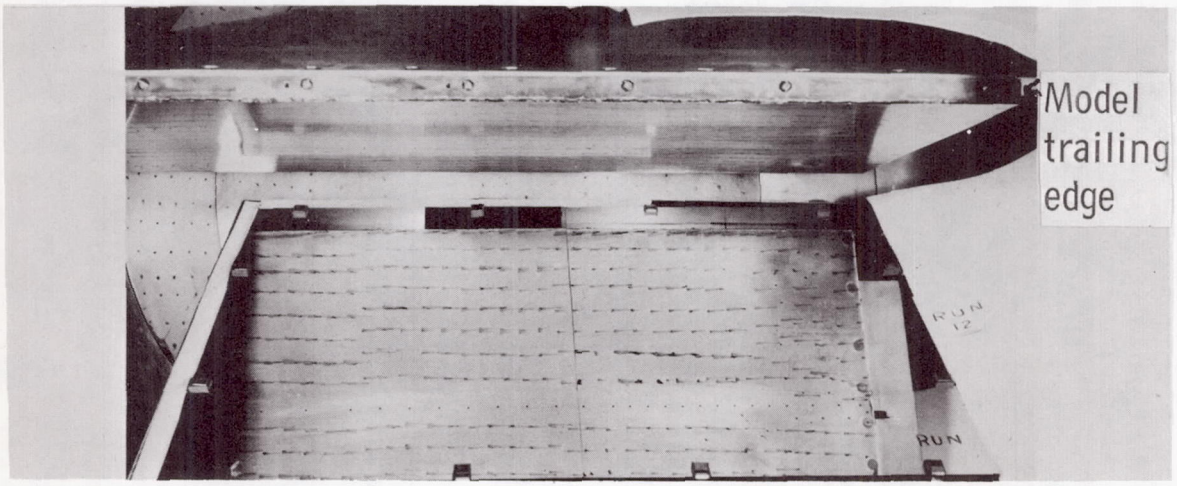

Rear portion of model

Figure 7.- Oil-flow patterns.

L-65-6253.1

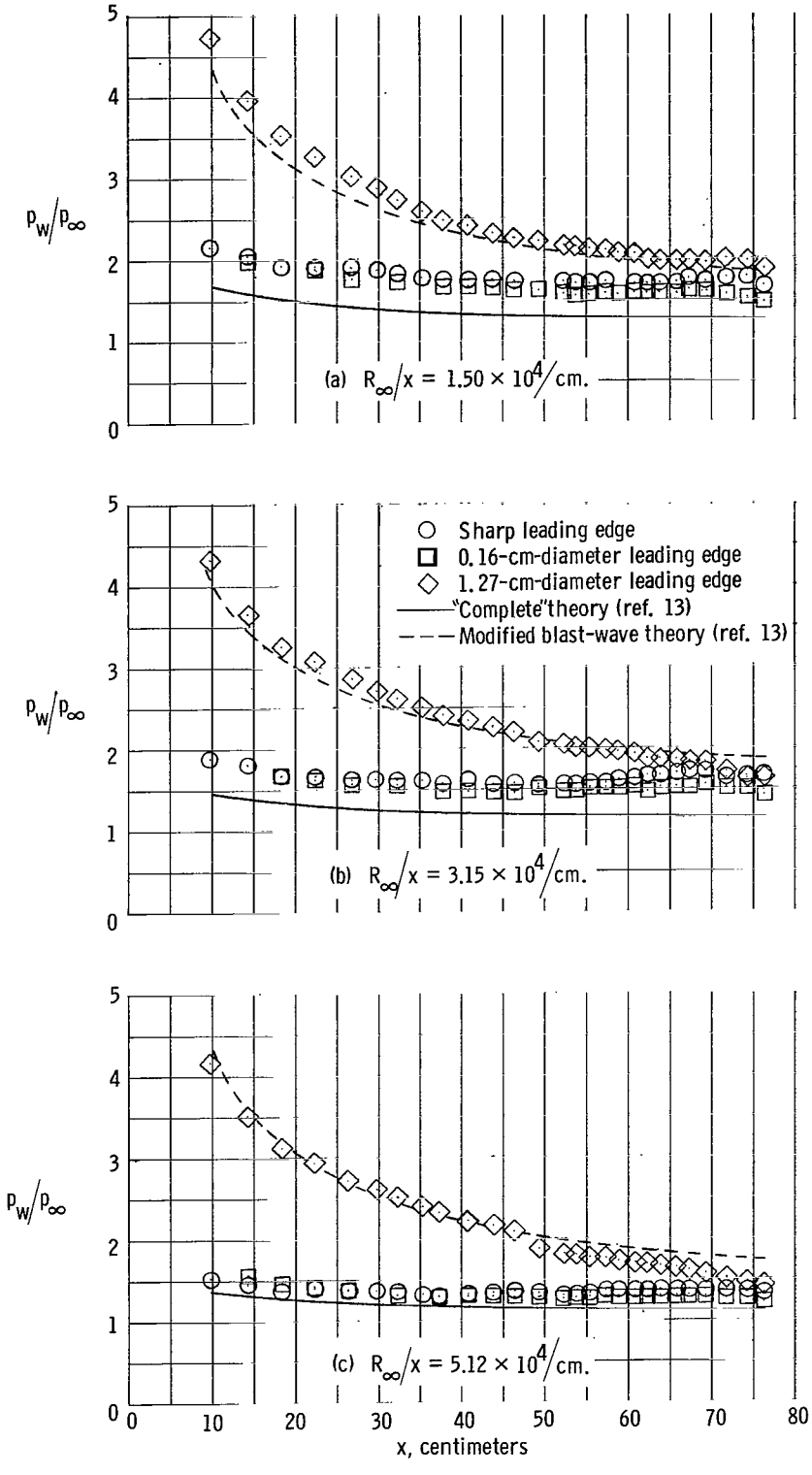

Figure 8.- Bluntness effects on wall-pressure distributions. $\frac{T_w}{T_t} \approx 0.34$.

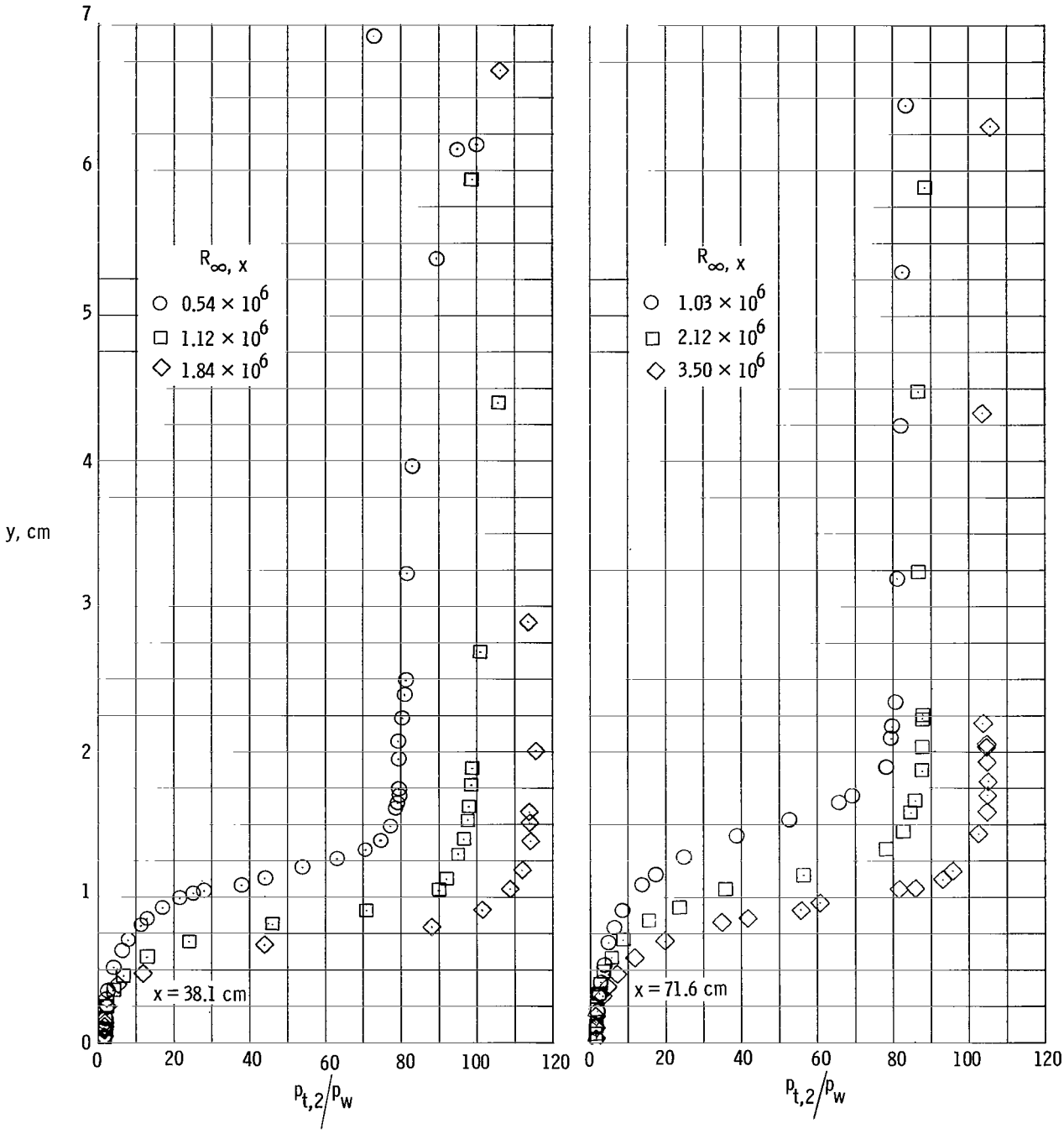

(a) Sharp leading edge.

Figure 9.- Impact-pressure profiles.

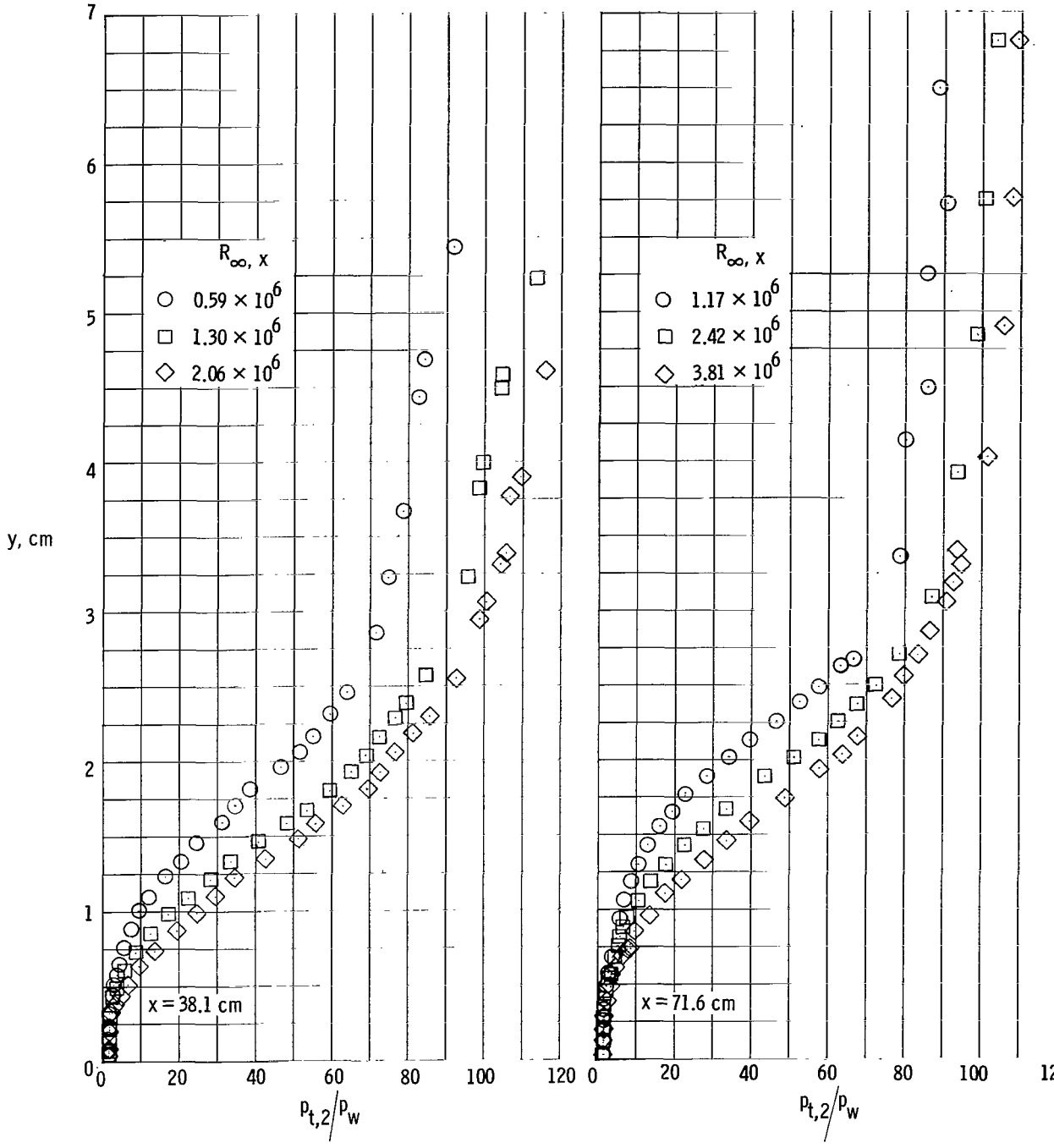

(b) d = 0.16 cm.

Figure 9.- Continued.

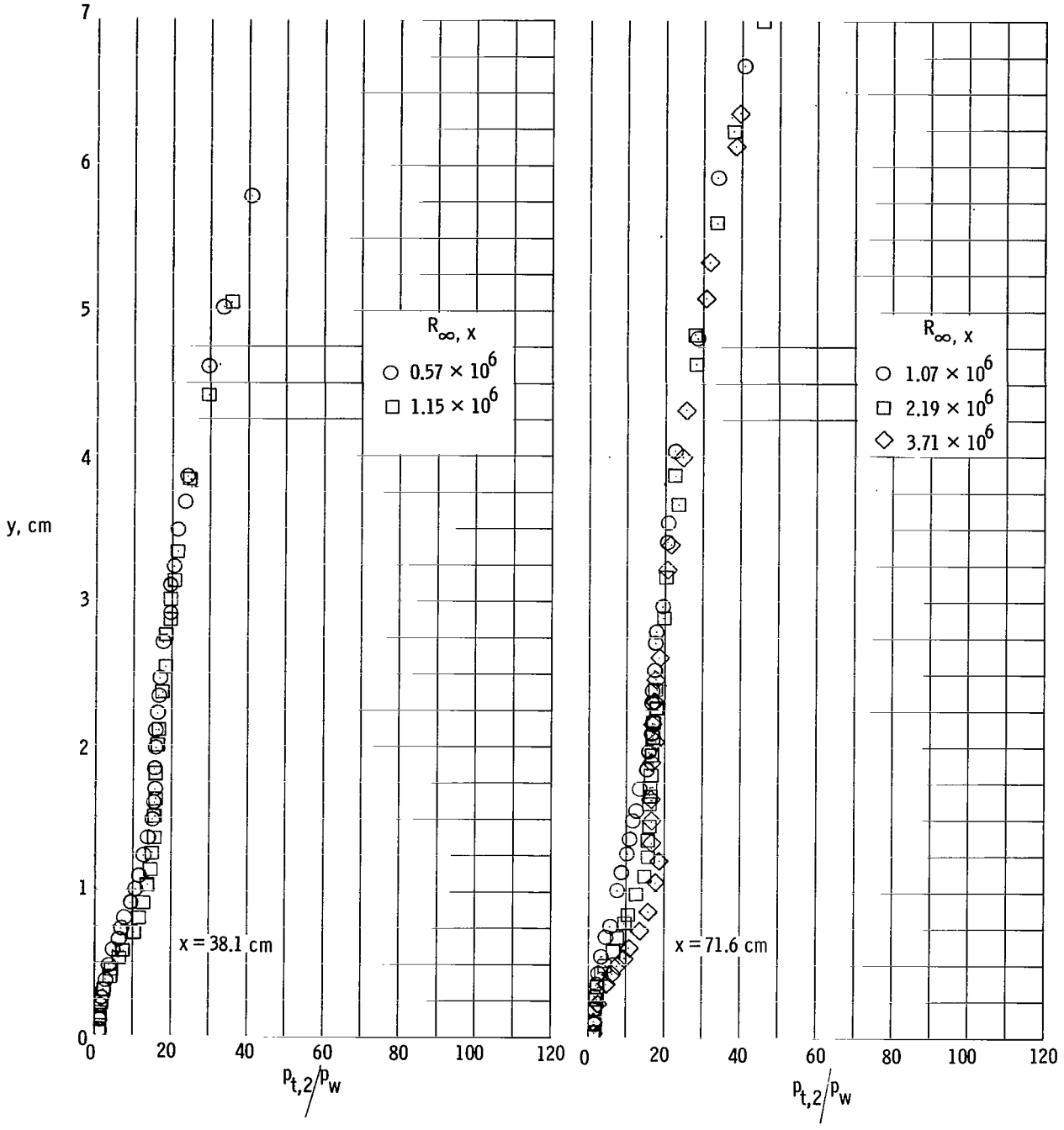

(c) d = 1.27 cm.

Figure 9.- Concluded.

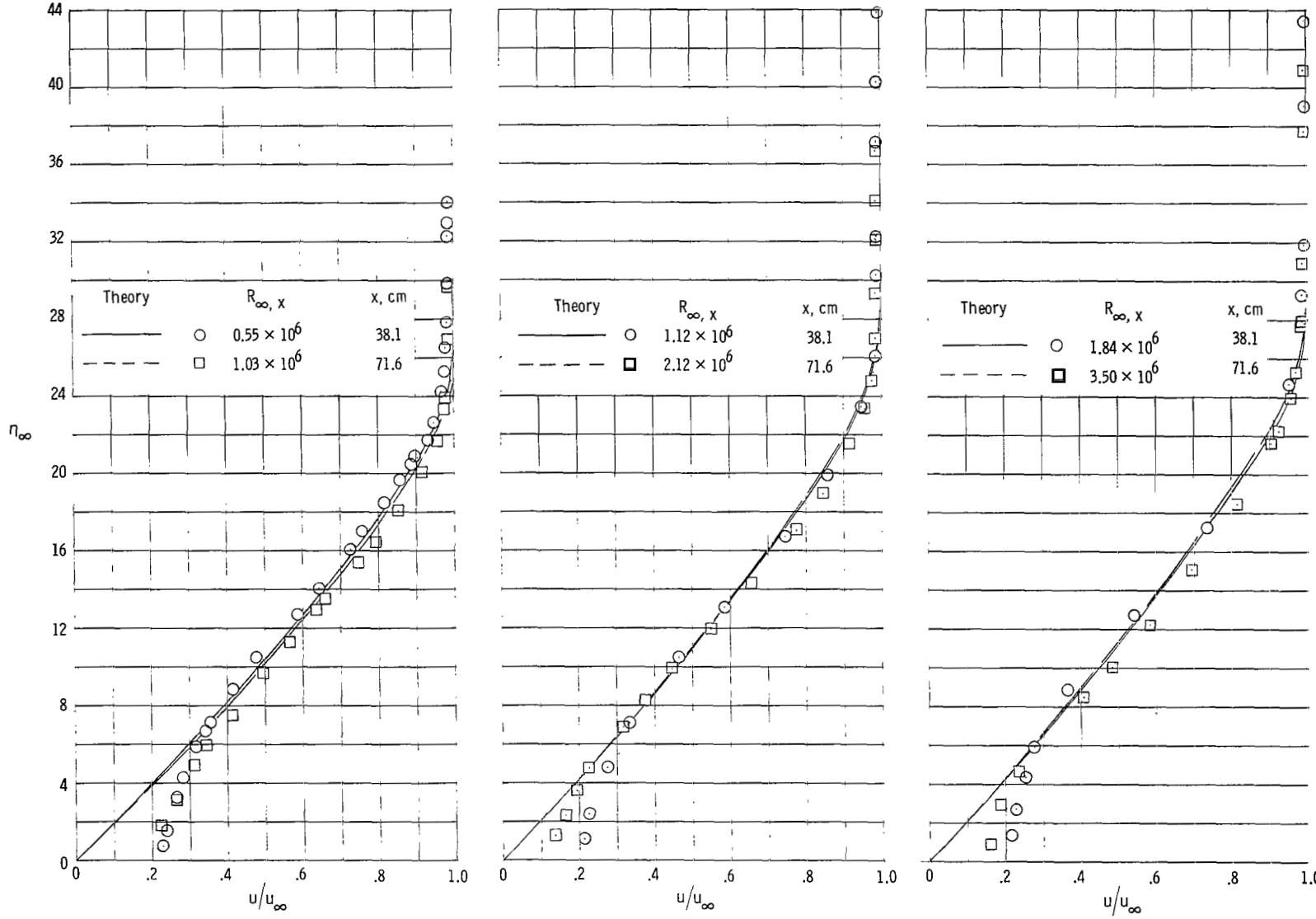

(a) $R_\infty/x = 1.42 \times 10^4$ cm.

(b) $R_\infty/x = 2.95 \times 10^4$ cm.

(c) $R_\infty/x = 4.84 \times 10^4$ cm.

Figure 10.- Velocity profiles for sharp-leading-edge model.

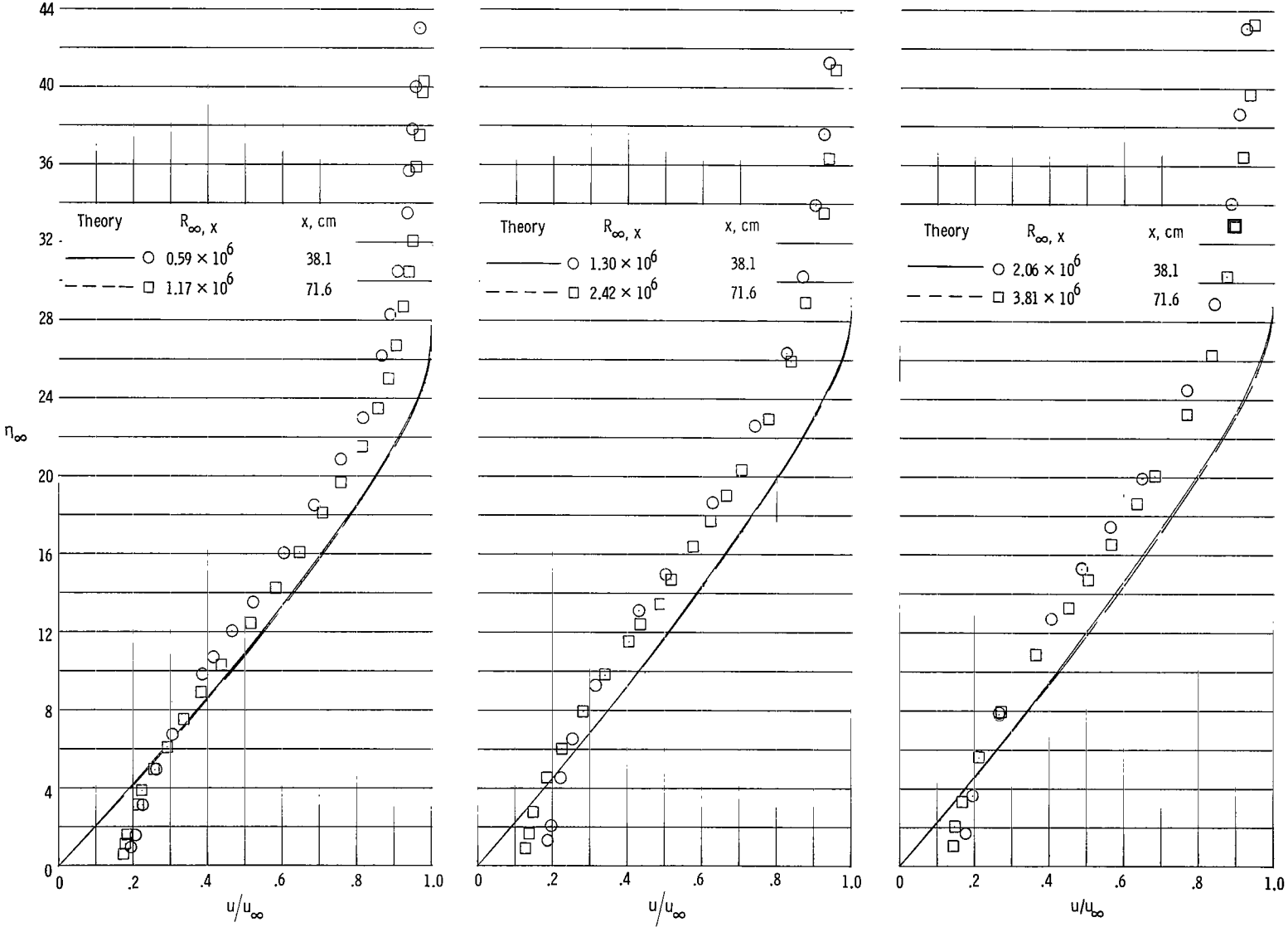

(a) $R_\infty/x = 1.61 \times 10^4$ cm.

(b) $R_\infty/x = 3.39 \times 10^4$ cm.

(c) $R_\infty/x = 5.35 \times 10^4$ cm.

Figure 11.- Velocity profiles for 0.16-cm-diameter leading-edge model.

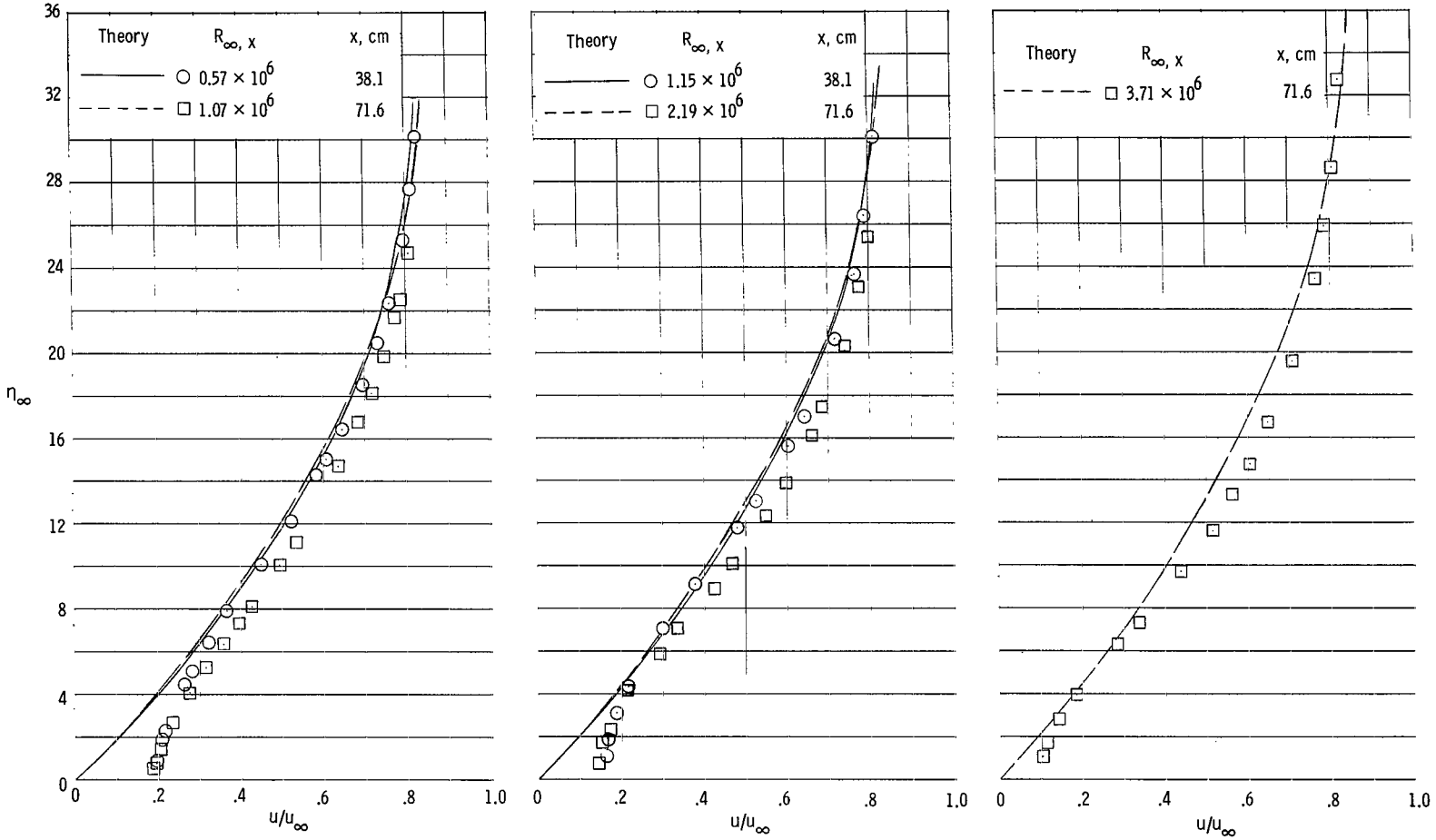

(a) $R_{\infty}/x = 1.50 \times 10^4$ cm.

(b) $R_{\infty}/x = 3.03 \times 10^4$ cm.

(c) $R_{\infty}/x = 5.20 \times 10^4$ cm.

Figure 12.- Velocity profiles for 1.27-cm-diameter leading-edge model.

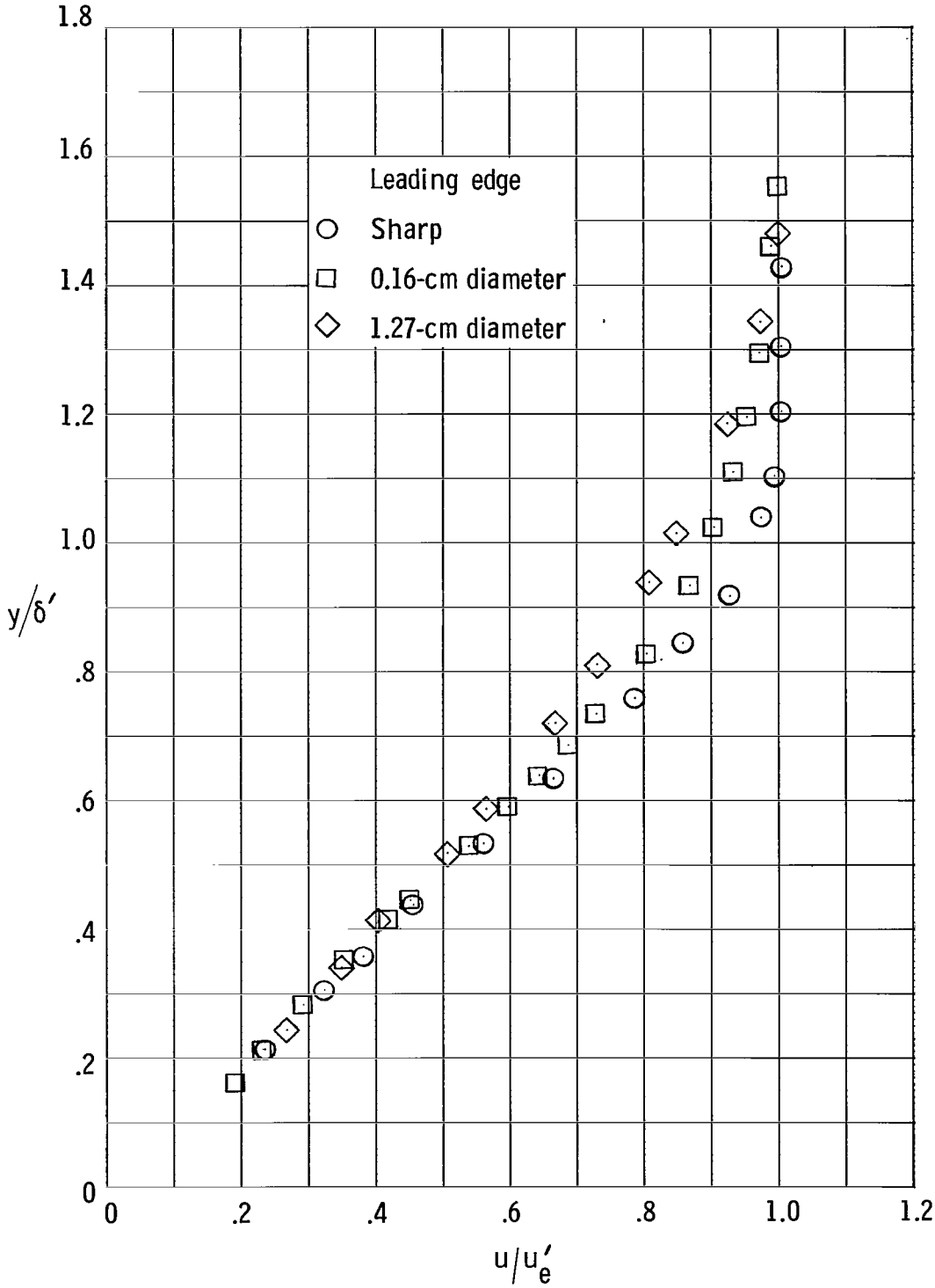

Figure 13.- Bluntness effect on velocity profiles. $x = 71.6$ cm; $R_{\infty,x} \approx 2.25 \times 10^6$.

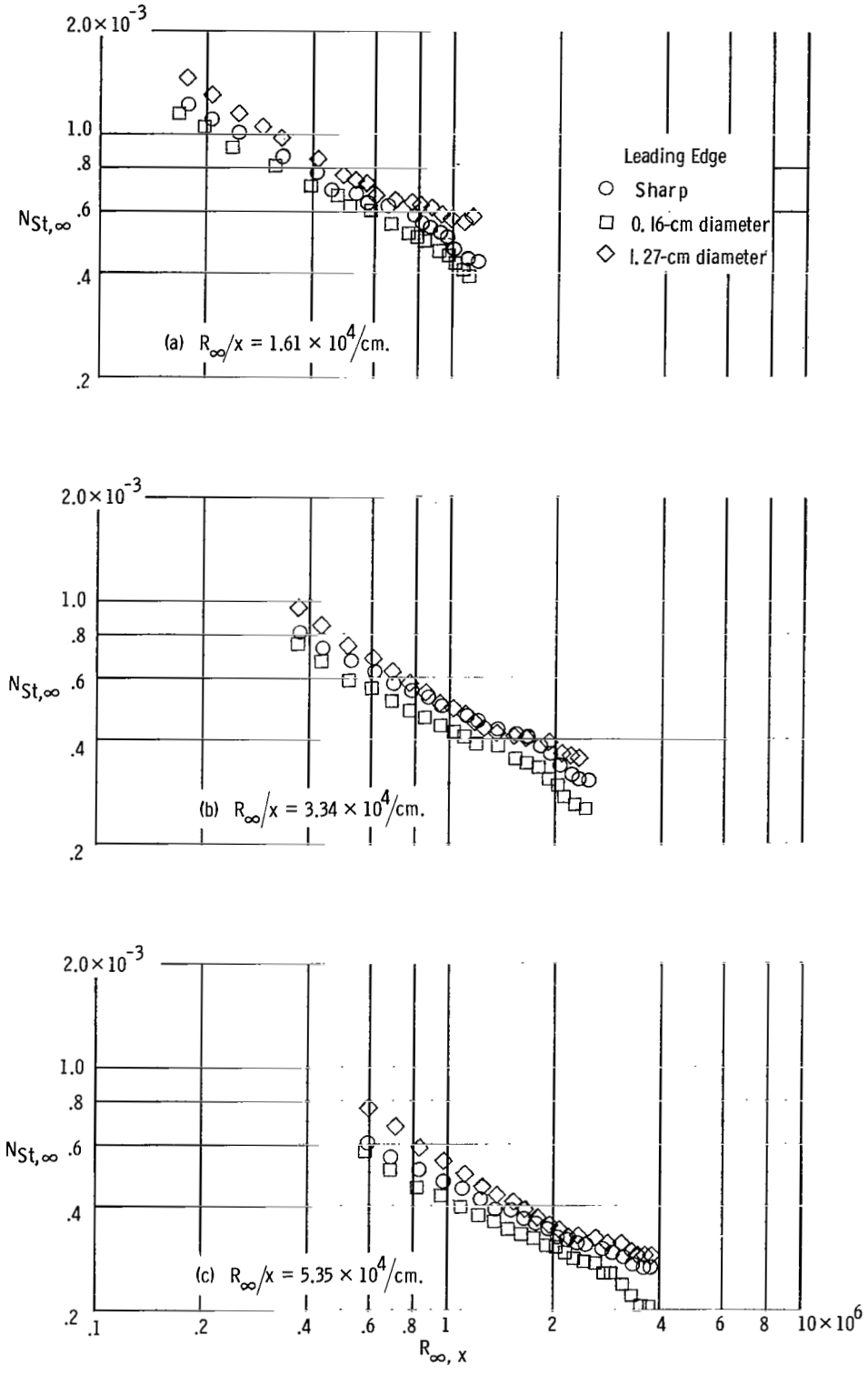

Figure 14.- Bluntness effect on heat transfer.

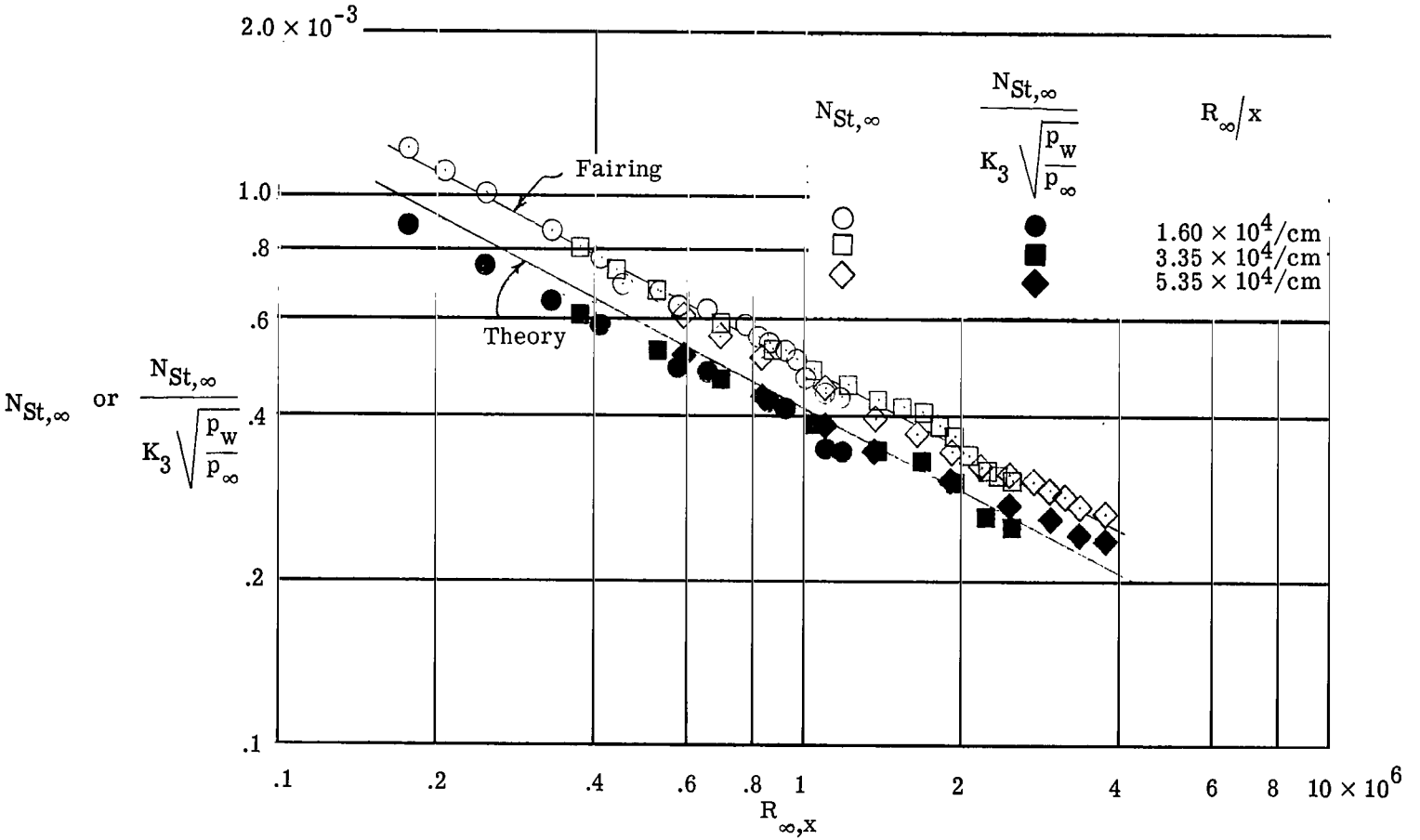

Figure 15.- Heat transfer to sharp-leading-edge model.

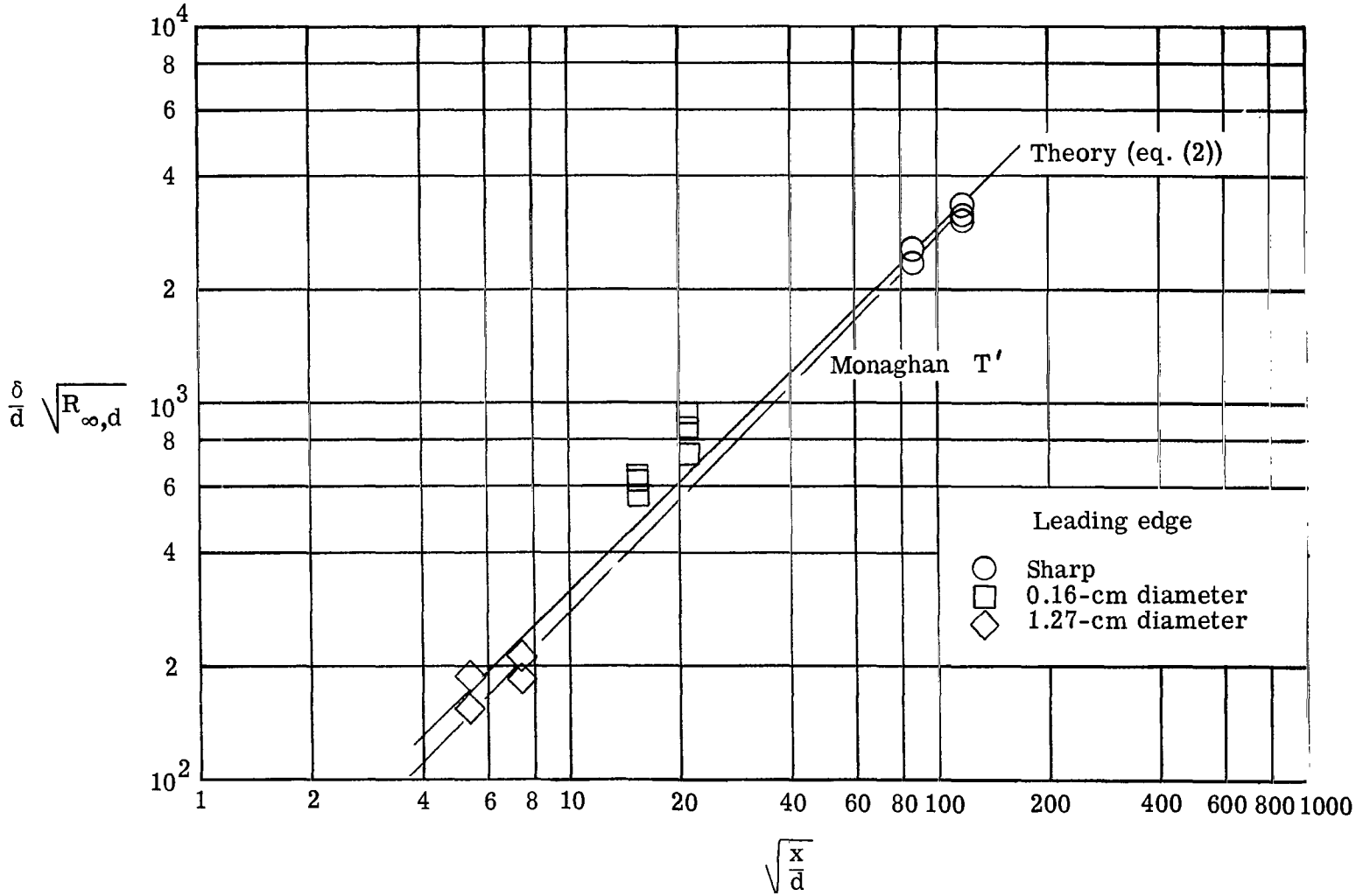

Figure 16.- Boundary-layer thickness behind different leading edges.

"The aeronautical and space activities of the United States shall be conducted so as to contribute . . . to the expansion of human knowledge of phenomena in the atmosphere and space. The Administration shall provide for the widest practicable and appropriate dissemination of information concerning its activities and the results thereof."

—NATIONAL AERONAUTICS AND SPACE ACT OF 1958

NASA SCIENTIFIC AND TECHNICAL PUBLICATIONS

TECHNICAL REPORTS: Scientific and technical information considered important, complete, and a lasting contribution to existing knowledge.

TECHNICAL NOTES: Information less broad in scope but nevertheless of importance as a contribution to existing knowledge.

TECHNICAL MEMORANDUMS: Information receiving limited distribution because of preliminary data, security classification, or other reasons.

CONTRACTOR REPORTS: Scientific and technical information generated under a NASA contract or grant and considered an important contribution to existing knowledge.

TECHNICAL TRANSLATIONS: Information published in a foreign language considered to merit NASA distribution in English.

SPECIAL PUBLICATIONS: Information derived from or of value to NASA activities. Publications include conference proceedings, monographs, data compilations, handbooks, sourcebooks, and special bibliographies.

TECHNOLOGY UTILIZATION PUBLICATIONS: Information on technology used by NASA that may be of particular interest in commercial and other non-aerospace applications. Publications include Tech Briefs, Technology Utilization Reports and Notes, and Technology Surveys.

Details on the availability of these publications may be obtained from:

SCIENTIFIC AND TECHNICAL INFORMATION DIVISION

NATIONAL AERONAUTICS AND SPACE ADMINISTRATION

Washington, D.C. 20546